JOURNAL OF AIRCRAFT
Vol. 44, No. 5, September–October 2007

Streamwise Vorticity in Simple Mechanical Flapping Wings

YoungSun Hong* and Aaron Altman†
University of Dayton, Dayton, Ohio 45469

DOI: 10.2514/1.27824

The presence of streamwise vorticity in the vicinity of the wing tip contributes to lift in thin flat plate zero pitch angle flapping wings in quiescent air. In creating flapping wing micro air vehicles it is desirable to maintain only the mechanical and kinematic complexity absolutely necessary to artificially duplicate flapping wing flight. This study quantifies the lift generated from a flapping motion of absolute minimum complexity thought to be capable of generating lift. Using a flapping wing micro air vehicle with wings fabricated in-house, streamwise vortices were identified along the span of wings of various aspect ratios and at numerous different points throughout the flapping cycle under a variety of operating conditions. The lift generated by the flapping mechanism was quantified experimentally using a force transducer and a high speed camera. Digital particle image velocimetry was used to determine the contributions of streamwise vorticity to the total measured lift. Further evidence was found of the importance of the relationship between wing span and flapping frequency in the nature of the formation and shedding of vortices.

Nomenclature

D = drag force
f = wing beat frequency
I = unit tensor
L = lift force
l = wing length
T = stress tensor
T^* = normalized time (temporal location in the flapping cycle * flapping frequency)
U_0 = velocity field into freestream
u = velocity
u' = perturbation components where $u = U_0 + u'$
x = position vector from the center of the body to the location of vorticity
α = angular acceleration
Γ_z = circulation about the z axis
Φ = wing beat amplitude (peak to peak, in radians)
ω = angular velocity
ω_z = vorticity vector in two-dimensional flow about the z axis

I. Introduction

FIXED wing micro air vehicles (MAVs) have been sufficiently investigated to the point where their operational limitations and opportunities for growth are well understood. The areas of gust tolerance and maneuverability, in particular, are rather limiting. These limitations have spurred interest in flapping and rotary wing MAV development. A number of commercial "ornithopters" are available for purchase, and several others have been developed at academic institutions. In general, these ornithopters offer limited range and payload and are incapable of hover. The process used to arrive at the store-bought ornithopter designs is proprietary and the development is often based on a trial and error approach to optimization.

Much work has been published in an effort to better understand both bird and insect flight. Most efforts focus on deconstructing bird and insect kinematic motion into its constitutive elements and deducing or measuring the aerodynamic effects of these motions. At a recent U.S. Air Force Office of Scientific Research (AFOSR) sponsored workshop on biologically inspired flight for MAVs [1], a consensus was reached among numerous experts in flapping wing fluid physics that in the process of studying animal flight, and in the creation of commercial ornithopters, some fundamental questions have yet to be answered. It was the recommendation of the workshop fluid physics group from the perspective of flapping wing MAV development that a set of "canonical" problems be developed from the simplest possible cases with complexity added to subsequent iterations. It was believed that these canonical problems could provide some context for the much more complex and unsteady aerodynamics associated with real animal flapping kinematics. One of the simple cases proposed for study was pure flapping in quiescent air which is the topic of the present study.

II. Lift from Vorticity

A. Lift from Vorticity over Fixed Wings

Leading-edge vortices that are produced in the well-studied case of delta wings induce a field of low pressure on the suction side of the wing. Such effects have been found to be tremendously effective in lift augmentation at low speeds and in unsteady flows (Taylor et al. [2]). However, swept wing research, and more specifically delta wing research, has for the most part focused on the disadvantages of and the problems associated with vortex effects on lift. As demonstrated in Fig. 1, in many instances, a vortex held or trapped above other types of lifting surfaces has been shown to generate lift [3,4]. Similarly, Kasper (Cox) [5] and Rossow [6] have also suggested a method to generate and maintain vortices on the upper surface of high aspect ratio wings.

B. Lift from Vorticity over Flapping Wings

A recurring theme in the flapping wing literature is the importance of understanding vortex shedding and how the vortices behave when they separate from the moving surface that created them. In flapping flight, birds and insects can modify wing beat amplitude, stroke angle, wing planform area (birds), angle of attack, and to a lesser extent flapping frequency to optimize the generation of vortices.

In flapping wings, several unsteady effects are thought to use circulation to augment lift force. One of these is a rotational mechanism termed *clap and fling* (Weis-Fogh [7]) and can be seen in Fig. 2a. The wings clap together at the end of the upstroke and peel apart at the beginning of the downstroke, rotating about their trailing

Presented as Paper 0448 at the Applied Aerodynamics Conference, San Francisco, CA, 5–8 June 2006; received 14 September 2006; accepted for publication 1 May 2007.

*Graduate Student, Department of Mechanical and Aerospace Engineering, currently a Korean Air Force Major.

†Assistant Professor, Department of Mechanical and Aerospace Engineering, 300 College Park Drive. Senior Member AIAA.

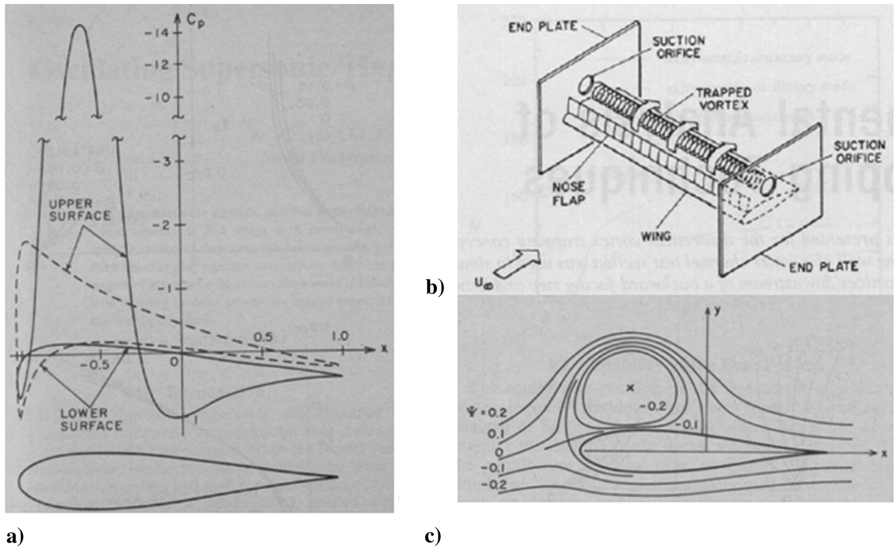

Fig. 1 Lift augmentation by trapping of a vortex (Riddle et al. [4], Huang and Chow [28]). a) Pressure distribution along the airfoil (dashed line represents baseline, no flap, case); b) trapped vortex over the airfoil; c) trapping of a vortex by a Joukowski airfoil.

edges and producing an initial strong bound vortex on each wing of equal and opposite sign. This fling-induced circulation can be large for high rotational velocities and enhances the downstroke lift. *Rotational circulation* (Dickinson et al. [8]) results from the interaction of translational and rotational velocity of the wing (Fig. 2b). *Wake capture* (Birch and Dickinson [9]) is a result of the interaction of the wing, when it inverts its motion, with the wake generated in the previous stroke (Fig. 2c). The wing benefits from the shed vorticity of the previous stroke.

Although wake capture is likely occurring in the experiments performed for this research, its effects will not be isolated. *Delayed stall* (Dickinson and Götz [10]) is the result of the translational motion of the wing and it depends only on the wing translational velocity and angle of attack (Fig. 2d). Delayed stall causes the formation of a leading-edge vortex (LEV) that reduces pressure over the wing and this phenomenon is considered the most directly relevant to the present research.

Delayed stall and the LEV can produce flow velocity magnitudes in the spanwise direction of the same or greater magnitude than flow velocities in the streamwise direction. These large spanwise velocities are often in the form of axial flow in the core of the vortex [11,12]. This flow characteristic has been largely ignored with the exception of its suspected contribution to the stabilization of the leading-edge vortex.

Changing the focus from the chordwise to the spanwise plane, other research has demonstrated that vortices on the wing tip contribute to the generation of aerodynamic force in some fixed and flapping wings [9,13]. Generally, the flapping wing vortices and their influence have been divided into three distinct regions: the tip vortex, the leading-edge vortex, and an interaction zone [14] (see Fig. 3).

During the latter half of the downstroke, the core of the leading-edge vortex breaks down at 60–70% of the wing span and separates from the wing. The separated vortex feeds into a large tip vortex. The tip vortex runs back to the starting vortex shed at the beginning of the downstroke. In flapping insects, the leading-edge vortex also runs along each wing to the wing tip, where it rotates to form the wing tip trailing vortex [15].

These wing tip vortices in the spanwise plane (streamwise vorticity) during the downstroke of the flapping motion might influence the generation of lift force. Maxworthy [16] identified the presence of the wing tip vortex with a flapping mechanism in a tank of glycerine (Fig. 4). These vortices were entirely responsible for the

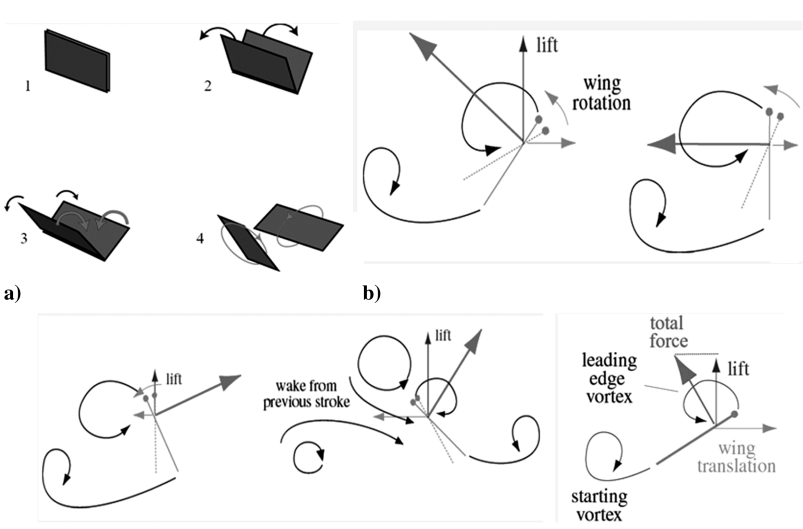

Fig. 2 Unsteady aerodynamics of flapping wings (Anders [29]). a) Clap and fling: the wings clap together at the end of the upstroke and peel apart at the beginning of the downstroke. b) Rotational circulation: the insect rotates its wings (dotted lines) creating a vortex, resulting in a propulsive force (left). c) Wake capture: the insect rotates its wing (dotted lines) and then the wing intersects its own wake and captures its energy in the form of lift (right). d) Delayed stall: causes the formation of a leading-edge vortex that reduces pressure over the wing.

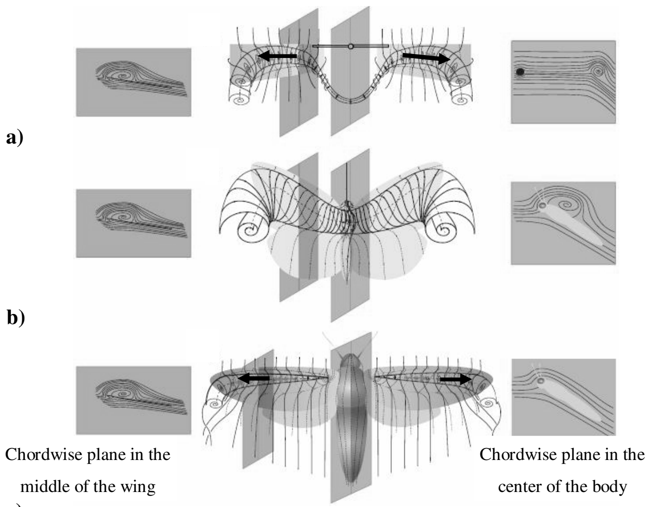

Fig. 3 The three classes of leading-edge vortex (LEV) and tip vortex (Bomphrey et al. [13]). a) The Maxworthy [30] model; b) the structure described by Luttges [31]; c) the structure described by Ellington [12] and Van den Berg [32]. Spanwise (axial) flow is marked by arrows in each case. Vertical planes show simplified flow topology at the centerline and midwing positions.

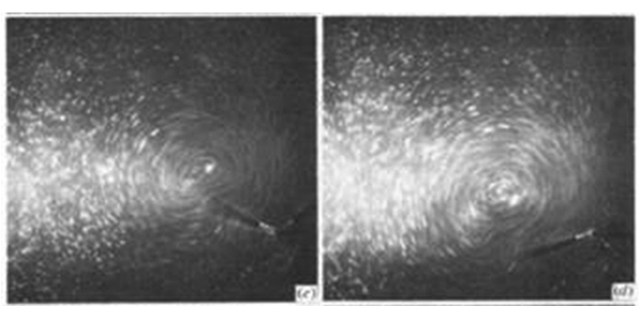

Fig. 4 Streamwise vorticity over a flapping mechanism in a tank of glycerine (Maxworthy [16]).

lift on the wings. Warrick et al. [17] mention that the tip vortices in hovering can even support the body weight of hummingbirds.

This study was performed first to identify the presence or absence of large-scale streamwise vortices in a kinematically simple flapping motion. If the presence of these vortices is identified, the order of magnitude of their contribution to the aerodynamic force will be determined. Temporal variation of the vortex force will be discussed and the influence of wing geometry on vortex formation and shedding is included.

III. Experimental Approach

In an effort to reduce the problem to its simplest form and isolate the effects of streamwise vorticity, flat plate wings were given a motion that can best be described as single hinged pure flapping (downstroke and upstroke) with no flapping stroke plane inclination angle. The chordwise pitch angle was fixed at zero degrees, or perfectly horizontal as viewed from the tip. The experiments were performed in quiescent air (no freestream velocity). In addition, this particular experimental setup guarantees that the origins of any vorticity creation or vortex shedding are independent of freestream influence and are due explicitly to the pure flapping motion itself. No effort was made to isolate the effects of wake capture as the study was intended only to identify the contributions of streamwise circulation and not necessarily isolate every possible contributor to the origins or interactions of this circulation.

To determine the magnitude of the contribution of streamwise vorticity to the total aerodynamic force, the total aerodynamic force was first isolated and quantified. The total force generated was measured with a force transducer. Inertial and added mass effects were then considered. The procedure will be explained further in the next section.

One method of determining the inertial contributions in flapping wings includes a vacuum container and a brass rod substituting for the uniform wing. An accelerometer can also measure the force due to the mass of wing at the mechanism's body center as shown by Bilo et al. [18]. The inertial force produced by the motion of the wing cannot accelerate the mechanism's center of mass. Sane and Dickinson [19] used the blade element method to estimate the inertial forces and Singh et al. [20] developed theoretical methods to calculate the inertial force. In this experiment, a high frame rate camera was used to take images of the flapping mechanism/wing using a fixed frame rate (constant time interval between images).

With an isolated aerodynamic force, digital particle image velocimetry (DPIV) was used to determine velocity and vorticity distributions over the wing. Circulation was calculated from the vorticity and was subsequently used to estimate lift force due to streamwise vorticity. Wing tip vortex flow visualization during the beginning and middle of the downstroke under various conditions was also included to provide a visual context for these phenomena.

A. Experimental Setup

The total lift force was measured using an Interface SSM-A5-250 "S" beam force transducer with a maximum error of 0.025 lbs, a maximum nonrepeatability of less than 0.02%, and a maximum creep in 20 min of less than 0.025%. The net aerodynamic force is determined from this measured total force by subtracting the experimentally determined inertial contribution. A high frame rate camera (FASTCAM—Ultima ADX-1000 frame/s) was used to permit experimental determination of the inertial forces of the flapping mechanism.

The inertial force is defined as the force due to mass and acceleration of the flapping mechanism, and it can be obtained using Newton's second law ($F = ma$). Angular velocity and angular acceleration were obtained by analyzing these images. The forces in the x and y directions of the flapping mechanism are calculated using angular velocity and angular acceleration and assuming uniform mass distribution.

$$\omega = \frac{\Delta\theta}{\Delta t} \tag{1a}$$

$$\alpha = \frac{\Delta\omega}{\Delta t} \tag{1b}$$

$$V_T = r\omega \tag{1c}$$

$$a_T = r\alpha \tag{1d}$$

where V_T and a_T are the tangential velocity and acceleration of the wings, respectively.

Flapping angles are then used to generate the inertial force distribution from a set of experimentally determined discrete points. To obtain the inertial force variation, the smoothed flapping angle distribution was approximated with a polynomial curve fit of order greater than 2. Then, using $F = m \cdot a$ and Eq. (1), the inertial force in the y axis (the axis aligned with lift and gravity) is obtained.

Sane and Dickinson's [19] treatment of added mass inertia for an infinitesimally thin two-dimensional plate in an inviscid fluid determined that for their experimental setup added mass effects were relatively small. Although they were using dissimilar kinematics to those used in this study, there were regions where the motion was similar. In the regions where linear velocity of the wing was not constant, the contributions of added mass inertia were still quite

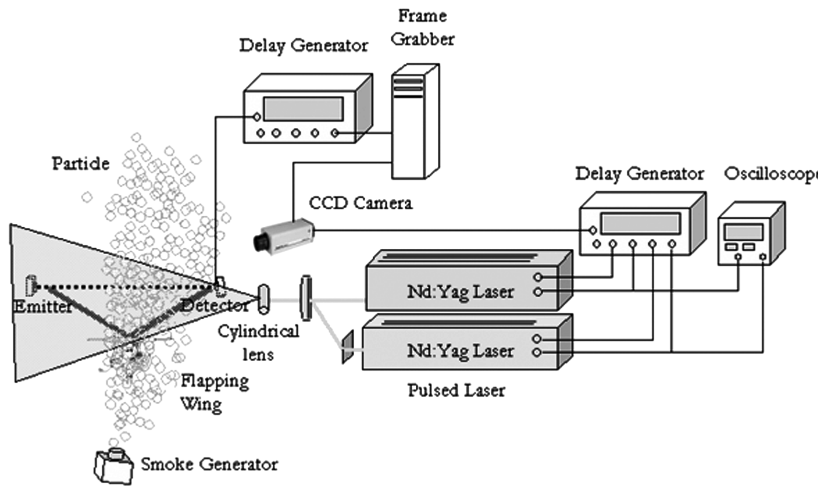

Fig. 5 PIV system setup.

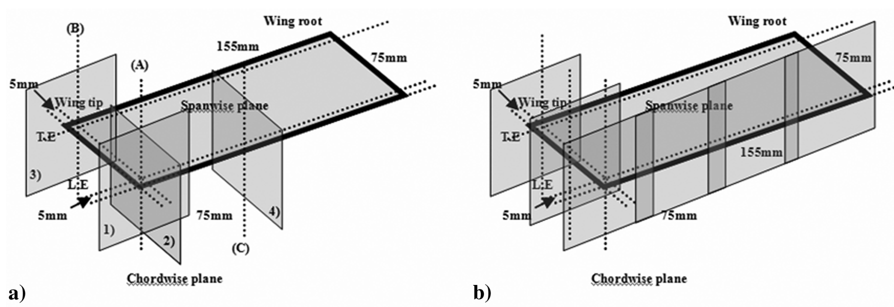

Fig. 6 PIV image planes. a) The spanwise plane at leading edge 1) and trailing edge 3) and chordwise plane at the wing tip 2) and middle of the wing 4) are considered. The dotted vertical lines indicate intersections between planes where the velocities perpendicular to the wing surface in both images should be the same. b) PIV image plane composite used to image the entire wing. The composite image plane was taken at a distance of 5 mm from the wing edge.

small. In addition, their study was performed in mineral oil with a density several orders of magnitude greater than air. Because the effort in the research presented in this paper was focused specifically on determining the relative magnitude of the vortex contribution to the overall lift force rather than an exact accounting of all measured force, it is reasonable to consider the effects of added mass inertia to be some small component contained within the resulting aerodynamic force component.

Figure 5 shows the DPIV setup for the experiment. A Megaplus ES 1.0 camera was used operating in the "frame-straddling" mode of image acquisition required for short interframe times required for PIV image acquisition. The camera synchronization with the frame grabber (EPIX) and laser firing (Spectra Physics, double pulsed 300 mJ/pulse 10 pulse/s Nd:YAG) is controlled via the strobe signal of the camera. The delay generator (Stanford Research DG 535) was used to trigger the PIV laser flash lamps and Q switches. The pulse that sends a signal starts all of the timing events and is in phase with the laser repetition rate. The trigger pulse from the flapping motion is used to trigger the camera. To trigger the pulse using the flapping motion, an emitter and detector are installed aligned with the peak of the flapping motion. When the flapping wings interrupt the beam, the detector produces a regular signal. The laser beam used for PIV is split through a cylindrical lens to generate the light sheet. The light scattered by the smoke particles (0.2–2 μm) is recorded on a 1 k $\times$ 1 k 8-bit progressive scan charge-coupled device (CCD) camera using a 25 mm Cosmicar C mount lens. The PIV images were taken at numerous locations along the span and at numerous chordwise stations (Fig. 6).

DPIV V2.0 [Innovative Scientific Solutions, Inc. (ISSI)] was used for postprocessing using a 64 pixel correlation size and a 50% image overlap. Image coverage was 4.3 cm $\times$ 4.3 cm, pulse separation time was 50 μs, and there was an average of 20 particles per interrogation region. Using the induced particle velocity method of Westerweel [21], and taking into consideration the maximum acceleration seen in the experiment, an error in velocity of less than 0.5% can be expected.

B. Flapping Mechanism and Wings

The flapping mechanism was adapted from a Cybird P1 remote control ornithopter model (Fig. 7a). The flapping mechanism is powered by a dc power supply. Depending upon the wing type, the operating angle was a weak function of flapping frequency. This was believed to result from lash in the mechanism but was not believed to have been significant enough to affect the predicted aerodynamic force once the inertial effects were removed. The frequency of 4 Hz

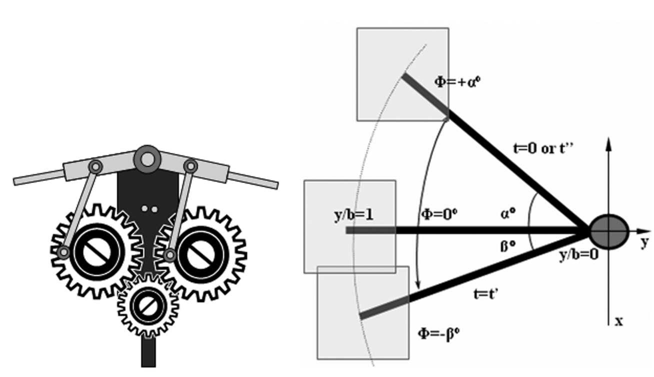

Fig. 7 a) The flapping mechanism; b) the coordinate system definition and the operating angle of the flapping mechanism. $\alpha = 41$ deg, $\beta = 18$ deg, $t' = 0.116$, $t'' = 0.134$ at a flapping frequency of 4 Hz with no. 4 wing. The shaded squares represent sample PIV image planes.

Table 1 Characteristics of the wings used in the experiment

Wing no.	Semispan, cm	Chord, cm	Aspect ratio	Mass
1	20	10	4	15.99 g
2	15	10	3	9.79 g
3	15	7.5	4	7.78 g
4	15.5	7.5	4.1	7.34 g
5	5.5	7.5	1.5	3.48 g

was selected from Alford and Altman [22] which demonstrated a strong correlation between span and flap frequency for flapping animals. The flapping frequency was set using a high precision strobe and remained constant to within roughly 1.5%. Table 1 shows the properties of the various wings used in the experiment. Figure 7b provides a reference coordinate system.

IV. Analytical Approach

A. Definition of Reynolds Number

Because there is some ambiguity in the literature regarding the definitions used for the Reynolds number (Re) in flapping wings the definition used is presented below for clarity. A mean Reynolds number for hovering flight based on the mean chord c ($=2l/AR$) and the mean wing tip velocity U ($=2\Phi f l$) has been defined as follows [23]:

$$Re = \frac{\rho c U}{\mu} = \frac{\rho \Phi f l^2}{\mu AR} \tag{2}$$

B. Computation of the Lift Force due to the Vortex

Lin and Rockwell [24] used a series of instantaneous patterns of vorticity obtained through PIV to calculate the force within a fixed visual frame. One formulation they cited was based on Lighthill's interpretation [25] where the vorticity to be included in force determination is the excess (shed) vorticity. For a two-dimensional, inviscid, incompressible flow, the instantaneous lift per unit length can be found using the following equation:

$$L = \frac{\mathrm{d}}{\mathrm{d}t}\rho\left[\left(\int_A x\omega_z \,\mathrm{d}A\right)\right] \tag{3}$$

To determine the effects of both sectional lift and drag forces from an instantaneous velocity field, Noca et al. [26] derived the following from the momentum equation:

$$F' = \rho \int_A u \times \omega_z \,\mathrm{d}A - \rho \oint_S n \cdot u(x \times \omega_z)\,\mathrm{d}S + \oint_S n \cdot [x \cdot (\nabla \cdot T)I - x(\nabla \cdot T) + T]\,\mathrm{d}S \tag{4}$$

When applying this equation to the determination of force production due to leading-edge vortices on flapping wings in a highly three-dimensional flowfield, Birch et al. [15] found that the sectional lift estimate based on circulation was contained within the first term in Eq. (4). They applied this term likewise in the determination of spanwise circulation. They expanded the first term into freestream and perturbation terms as follows:

$$\rho \int_A u \times \omega_z \,\mathrm{d}A = \rho U_0(z)\Gamma_z(z) - \rho \int_A u'\omega_z \,\mathrm{d}A \tag{5}$$

This term was referred by Noca et al. as the Kutta–Zhukovski (Joukowski) term. Birch et al. concluded that a large percentage of the lift experienced by the wing was due explicitly to the $\rho U_0(z)\Gamma_z(z)$ term. Most would recognize this term as the traditional result of the Kutta–Joukowski theorem commonly used in steady state to calculate the lift force directly from circulation. The unsteady result from Lin and Rockwell [24] [Eq. (3)] was reduced and applied similarly in the determination of lift force from circulation calculated from an instantaneous velocity field. A fixed control volume is selected in the inertial frame of reference around the wing to calculate the lift force generated.

To determine the magnitude of the contribution of the out-of-plane velocity, a number of chordwise planar slices were evaluated in the same locations as the spanwise planar slices used. Figure 8a shows representative flow features in the chordwise plane along with the velocity magnitudes. In general the velocity magnitudes were approximately 75% of those found in the spanwise plane and the flow features were considerably smaller. Figure 8a shows a result considered representative of the majority of chordwise images taken next to a representative spanwise image (Fig. 8a). If a complete accounting of the aerodynamic forces was going to be completed, the out-of-plane flow would need to be included in the analysis. The focus of the present research was on isolating the forces generated by vortical flow in the spanwise plane, however. An approach to decomposing a three-dimensional flowfield into chordwise and spanwise slices similar to that used by Birch et al. [15] was thus employed.

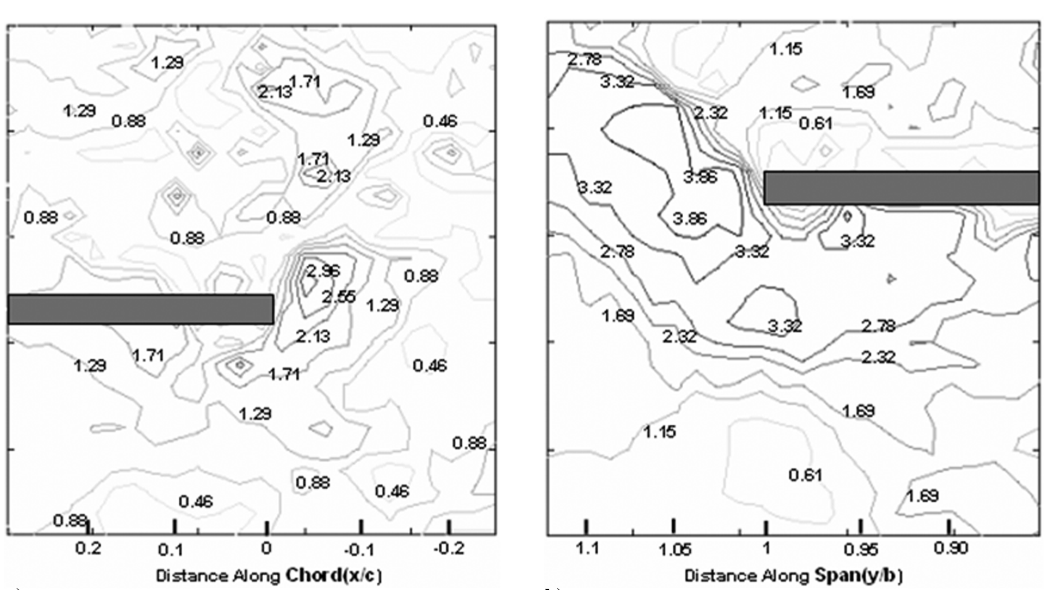

a) b)

Fig. 8 Speed distribution (in units of m/s) of the flapping wing in the start of the downstroke at 4 Hz with the no. 4 wing. a) Chordwise plane; b) spanwise plane (planes 1 and 2 in Fig. 6a) ($\phi = +31$ deg).

V. Results and Discussion

A. Time History of Flapping Motion

An example of flapping angle variation with time can be seen in Fig. 9a for the 4 Hz case (0.25 s period) with the no. 2 wing from Table 1. In this figure it is evident that there is a slight asymmetry in the flapping motion. The time spent in the downstroke is 0.116 s ($0 < T^* < 0.464$) leaving 0.134 s ($0.464 < T^* < 1$) in the upstroke. This yields average speeds of 1.91 and 1.52 m/s in the downstroke and upstroke, respectively, with maximum speeds of 3.7 and 2.8 m/s in the downstroke and upstroke, respectively. The effects of this asymmetry will be seen later in differences in the formation and shedding of vortices in the up- and downstrokes. Also in Fig. 9a the approximated curve fit can be seen superimposed over the experimental results. For the same (experimental) case, the tangential velocity calculated at the tip of the wing using the variation in flapping angle with time can be seen in Fig. 9b alongside a polynomial curve fit approximation. It was necessary to create a smoothed approximation curve to the tangential velocity due to the fact it was subsequently used to derive the acceleration. Figure 9c more clearly shows the relative time spent in the up- and downstrokes. The magnitude of the maximum velocity in the downstroke is clearly greater than in the upstroke. The tangential acceleration variation with time can be seen in Fig. 9d. As expected the maximum accelerations occur in the transitions from downstroke to upstroke and vice versa.

B. Force due to Inertia

Inertial forces shown here represent the acceleration force on the mass of the wing. The aforementioned representative results from the high frame rate camera are used to generate the inertial force distribution which is presented both in raw form and in the form of an approximated polynomial curve fit. Figure 10a shows the total lift force variation and the inertial force variation throughout the entire cycle from the beginning of the downstroke to the end of the upstroke for a typical data set. As is commonly cited in the literature, the inertial force is typically of the same order of magnitude as the aerodynamic force. These trends were observed for wing numbers 1, 2, and 3 at flapping frequencies of 3, 4, 5, and 6 Hz.

Figure 10b shows the resulting lift force contribution of the aerodynamic force in which the inertial force is subtracted from the total measured lift force. At the beginning of the downstroke and at the end of the upstroke, the inertial force is greater than the total measured force. This is due to a negative aerodynamic lift force (Fig. 10b) which cancels out the inertial contribution. It is noted that the trends for temporal variation in total aerodynamic lift force and measured total lift force are similar in shape throughout most of the flapping cycle.

It will be shown later that at the top of the downstroke a vortex is formed that is eventually shed in the downstroke. Although not seen in Fig. 10, occasionally there was a small increase in lift force at the stroke reversal. In these instances it is believed to be due to the shed vorticity impacting the wing (wake capture). As will also be discussed later, no large-scale streamwise vorticity was found to exist in the upstroke. Clearly the maximum acceleration in transition from downstroke to upstroke is considerably less than in the upstroke to downstroke transition. This is thought to have directly impacted the formation of vortices in these transitions.

C. Wing Parametric Study

Figure 11 shows results of a parametric study on wing dimensions. Comparing Figs. 11a and 11b shows that the total force for both frequencies and across all wings tested peaks early in the downstroke. At both frequencies the measured force due to the stroke

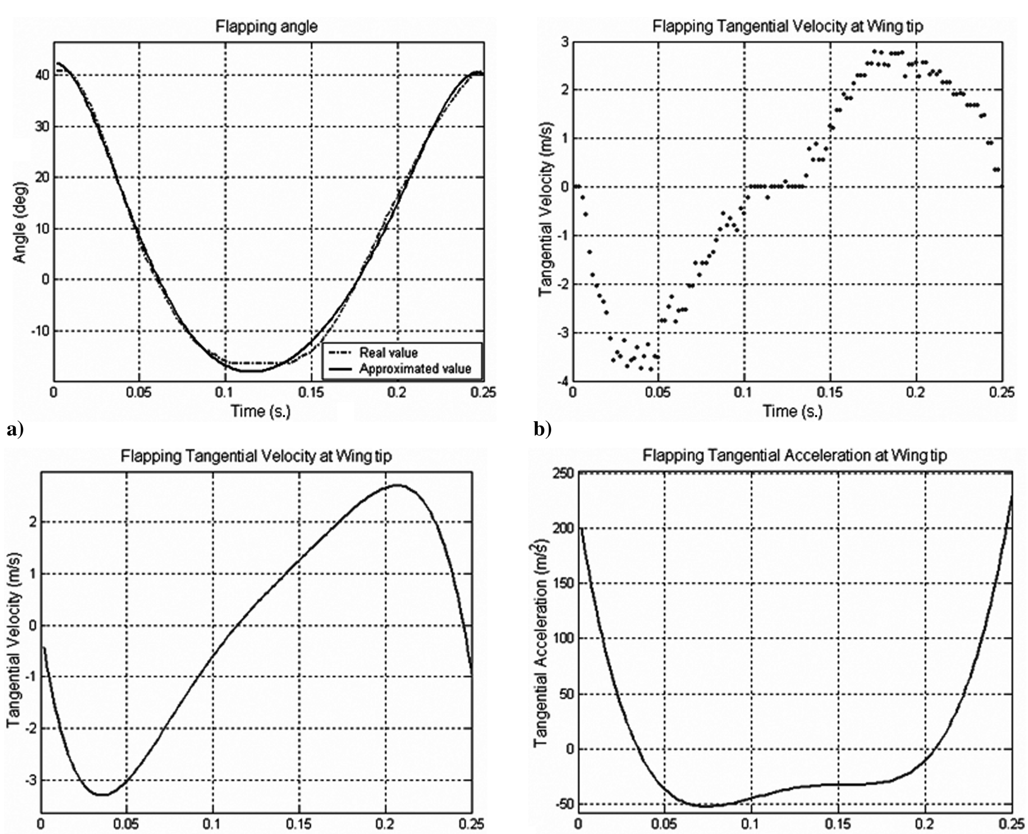

Fig. 9 The flapping angle, tangential velocity, and acceleration variation using real data and approximated data using wing no. 2 at a 4 Hz flapping frequency during one complete cycle. a) Flap angle variation; b) tangential velocity at the wing tip calculated using measured flap angle variation; c) the tangential velocity at the wing tip calculated using the approximated value of flapping angle variation; d) the tangential acceleration at the wing tip calculated using the approximated value of the flap angle variation.

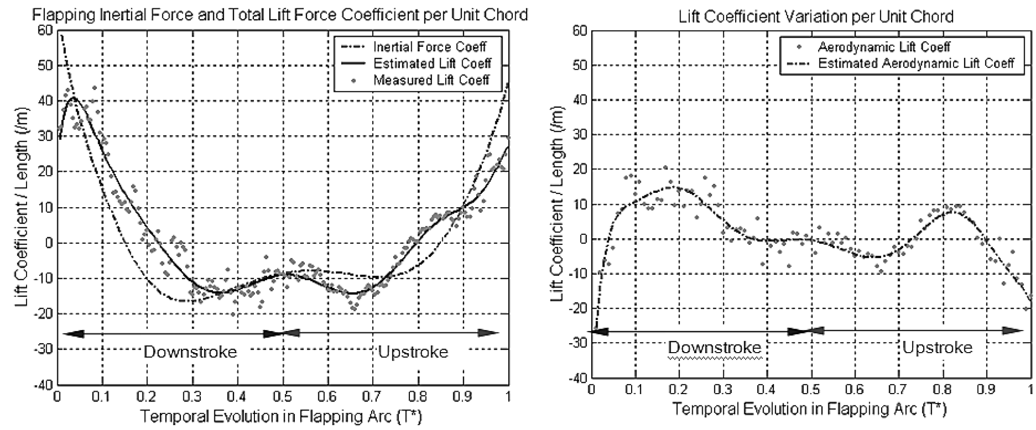

a) b)

Fig. 10 The temporal variation in force coefficient using wing no. 2 at a 5 Hz flapping frequency during one complete cycle. a) Total force coefficient including the inertia force coefficient and b) isolated aerodynamic force coefficient.

reversal is greatest for the largest wing. In addition, less time is spent in the downstroke than the upstroke for all cases. Figures 11c and 11d provide lift coefficient data that contrast the force results well. The overall shape of all normalized curves is quite similar. Most notable from the coefficient results is that the two smaller (span) wings generate peak lift coefficients at lower flapping frequency than the larger wing tested. There is no such correlation to the chord length. This result supports the previously identified correlation between flapping frequency and wing span found in nature [22] and provides more insight into the possible importance of geometry and flapping frequency in determining an optimal value of circulation for any given vortex [27].

D. Streamwise Vorticity

Figure 12 provides an example of one type of vortex production typically observed during testing. The figure shows a raw image of small-scale shed vortices during the downstroke alongside PIV results for vorticity. The noise rejection threshold for vorticity was on the order of 10%. Figure 13 shows the vorticity distribution and magnitude at two different flapping frequencies during the downstroke relative to the wing tip. The trajectory of the shed vortices is notably different across the two vorticity figures. In addition, it can be observed from the figures that the large-scale wing tip vortex was not generated during the downstroke at low frequency (for the large span wing). However, at the higher flapping

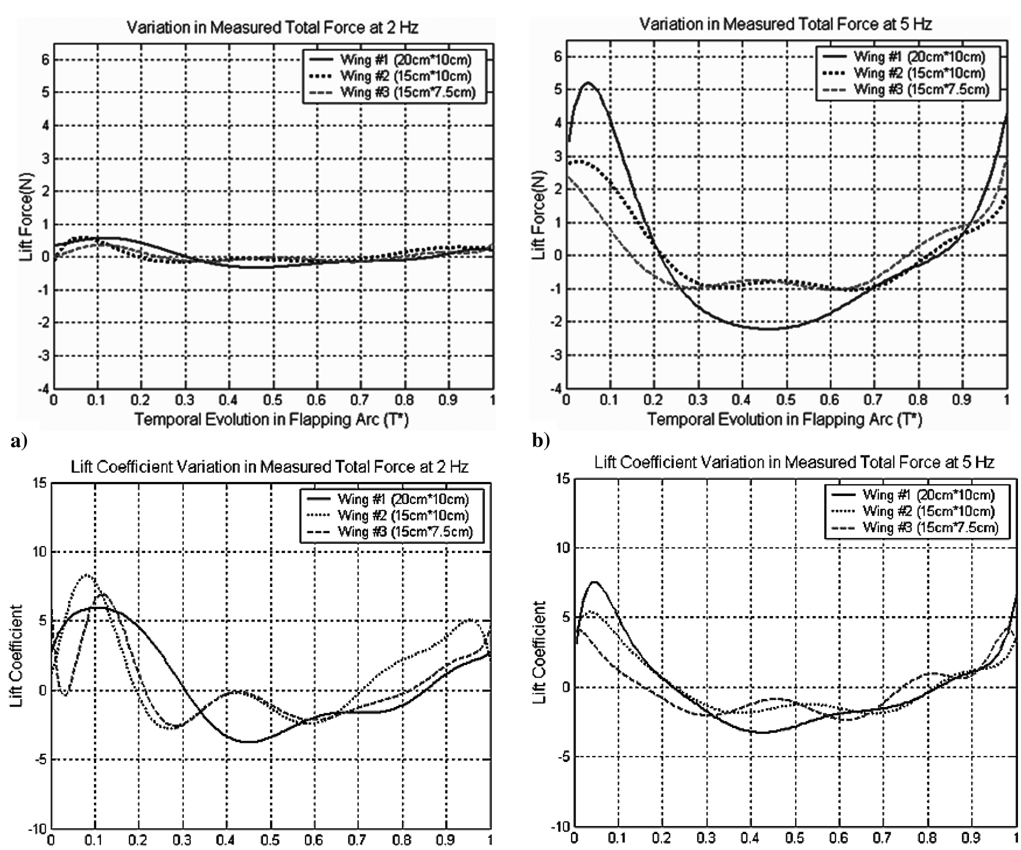

a) b) c) d)

Fig. 11 Temporal variation in the isolated lift force and lift coefficient for flapping wings of different dimensions. a) The time variation in total measured lift force of various wings at a flapping frequency of 2 Hz. b) The time variation in total measured lift force of various wings at a flapping frequency of 5 Hz. c) The time variation in lift coefficient of various wings at a flapping frequency of 2 Hz. d) The time variation in lift coefficient of various wings at a flapping frequency of 5 Hz.

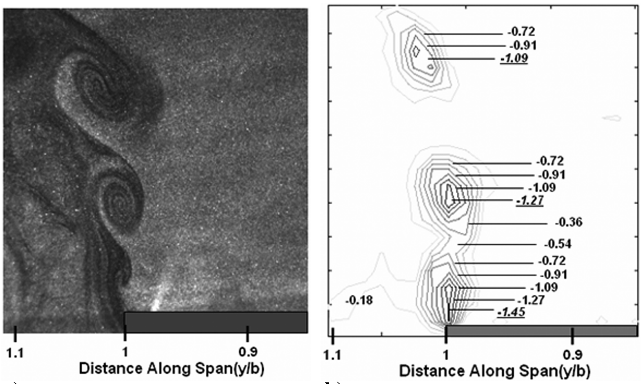

a) b)

Fig. 12 The no. 4 wing at $\phi = 28$ deg ($T^* = 0.027$) at the beginning of the downstroke at a 4 Hz flapping frequency. The chordwise location of the light sheet is 0.5 cm ($x/c = 0.067$) from the leading edge. a) Flow visualization; b) vorticity from image pair including a). The values denote vorticity (s^{-1}) ×1000.

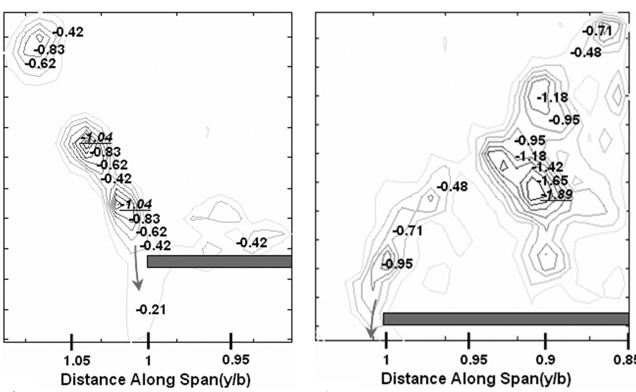

a) b)

Fig. 13 Vorticity distribution over the no. 1 wing in the middle of the downstroke at $\phi = 0$ deg and chordwise light sheet location of 0.5 cm ($x/c = 0.05$) from the leading edge. a) 4 Hz frequency with small-scale vortex shedding ($Re = 11,340$); b) 5 Hz frequency with the large-scale vortex present ($Re = 17,600$). The values denote vorticity (s^{-1}) ×1000.

frequencies tested well-formed large-scale wing tip vortices were generated.

Results from the present experiments show that the wing tip vortex is always seen early in the downstroke. However, the wing tip vortex was not seen during the upstroke. This is likely related to the asymmetry in the time history of the up- and downstrokes effecting formation of the vortices.

E. Vortex Force Coefficient Variation in the Downstroke

Figure 14 compares the magnitude of the vortex force early in the downstroke at 2 and 4 Hz flapping frequencies for the no. 4 wing. In yet another context, the smaller span wing can be observed generating a higher coefficient at a lower flapping frequency providing more evidence of a connection between optimal flapping frequency and wing planform geometry and the force generated due to circulation. The vortex force is gradually increasing as the stroke progresses for the duration of the flapping cycle included in Fig. 14.

Figure 15 is a case study for the vortex force coefficient distribution along the wing for the cases where the vortex is attached to the wing surface in the spanwise plane or shed from the wing in the middle of the downstroke. Figure 15a shows the lift coefficient distribution for the shed vortex case (4 Hz flapping frequency) and Fig. 15b shows the lift coefficient distribution for the large attached vortex case. The lift force available in the control volume [24] in vortex force coefficient form is $0.3646/\mathrm{m}$ (per meter of chord) when the large-scale attached vortex was present, compared to $0.1292/\mathrm{m}$ when smaller scale vortex shedding was occurring.

Figure 16 shows the calculated vortex force coefficient and vorticity as the flapping motion evolves early in the downstroke at a 2 Hz flapping frequency. Although there is scatter due to the instantaneous nature of the PIV image pairs used to determine the coefficients and forces, some clear trends can be observed. As the flapping motion progresses, the lift due to the vortex decreases slightly at the beginning of the downstroke. This decrease is thought to originate from the residual upward motion of the fluid during stroke reversal due to the low (relative) pressure of the fluid trailing behind the wing ultimately impacting the wing and subsequently detracting from the net force. The lift force due to the vortex increases again from the minimum value because the circulation increases as the downstroke evolves (Fig. 16, region B). The lift force decreases again from the maximum value because the vortices are shed or dissipate as the stroke evolves (Fig. 16a, region C). It is noted that for the values of lift force presented in all vortex derived lift figures, lift from only one wing is represented (vs two wings for measured aerodynamic force).

In another instance (Fig. 17 for wing no. 5 at a 4 Hz flapping frequency), the shape of the vortex lift coefficient variation throughout the flapping cycle (Fig. 17a) was markedly different when compared to the previous case (Fig. 16a). This difference is most likely due to the dramatic contrast in aspect ratio between the two cases. The wing used in Fig. 17 has a much lower aspect ratio due to a drastic reduction in span. Although the reduction in absolute span enabled DPIV evaluation of the entire wing semispan, the temporal variation of the vortex formation and shedding was quite different at the frequency shown. Whereas the vortex lift coefficient peaked at a T^* of approximately 0.09 in Fig. 16, the peak vortex lift coefficient in Fig. 17 can be seen closer to a T^* of approximately 0.06. Additionally, the suspected "wake capture" effects present in Fig. 16 appear to be absent in the results in Fig. 17.

VI. Conclusions

Thin flat plate zero pitch angle wings were flapped in quiescent air. In the process of investigating streamwise vorticity, a relationship was found to exist between wing span and flapping frequency in the

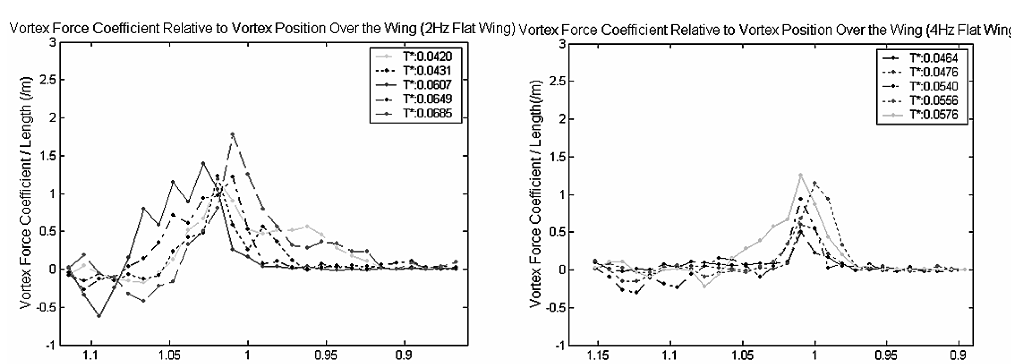

a) b)

Fig. 14 The spanwise vortex coefficient force distribution early in downstroke at a) 2 Hz frequency, $Re = 2680$ (no. 4 wing); b) 4 Hz frequency, $Re = 6310$ (no. 4 wing).

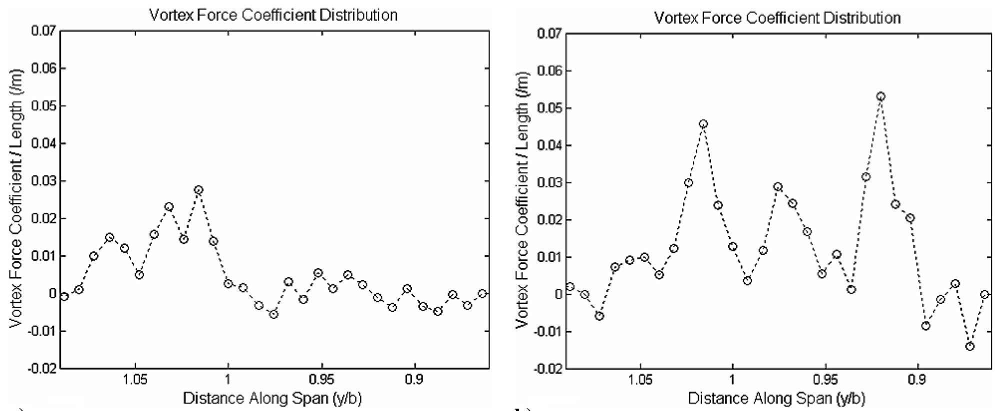

a) b)

Fig. 15 a), b) The distribution of the vortex force coefficient in the spanwise plane in the middle of the downstroke (with the no. 1 wing) at 4 Hz and 5 Hz flapping frequencies, respectively. The light sheet is 5 mm from the leading edge ($\phi = 0$ deg).

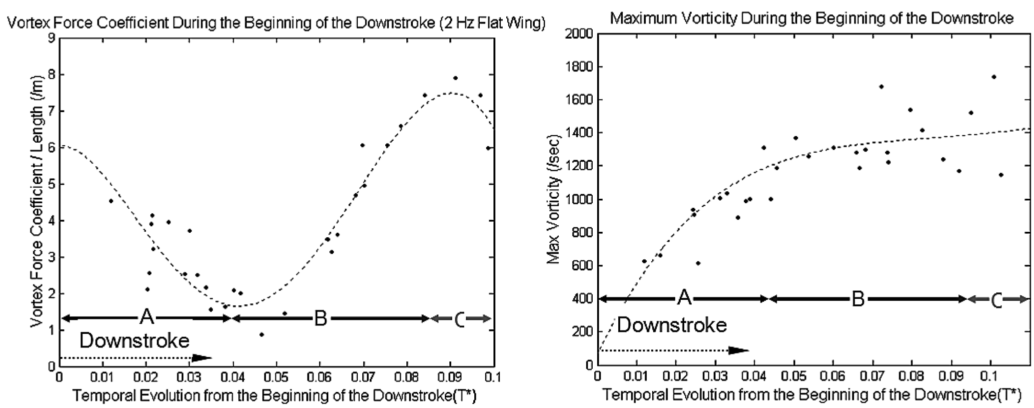

a) b)

Fig. 16 At a 2 Hz flapping frequency with the no. 4 wing. a) The vortex lift coefficient vs normalized time from the beginning of the downstroke; b) the maximum vorticity vs normalized time from the beginning of the downstroke. The points represent the vortex lift force coefficient variation calculated from the PIV results. The dotted lines represent the approximate lift force coefficient variation or maximum vorticity variation using a fifth degree polynomial.

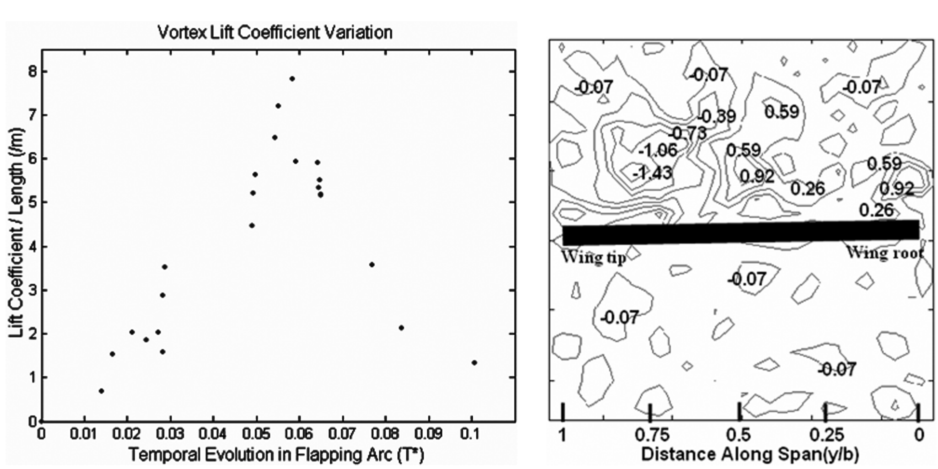

a) b)

Fig. 17 a) Vortex lift coefficient variation during the downstroke in the presence of the large-scale spanwise planar vortex b) instantaneous vorticity over the entire semispan ($\phi = -2$ deg). For a 4 Hz flapping frequency with the no. 5 wing, vorticity (s^{-1}) ×1000.

determination of the presence or absence of attached large-scale vortices. This result would appear to validate the concept of the existence of an optimal level of circulation a given vortex can accept before vortex separation occurs.

The presence of streamwise vorticity in the vicinity of the wing tip contributes to lift in thin flat plate zero pitch angle flapping wings in quiescent air. When isolated, inertial force contributions were found to be of the same order of magnitude as the aerodynamic force contributions. Aerodynamic force variation was compared for a number of wings of different aspect ratios. The aerodynamic force variations set the context for discussion of vortex force contributions. The effects of the parametric variations of wing aspect ratio on vortex formation and shedding and subsequently vortex force variation were discussed. The time-dependent force variation due to vortex development early in the downstroke was also shown for a number of different cases. There is still a great deal of knowledge to be obtained through continued study of the simple flapping motion in quiescent air alone as there are numerous variables (pitch angle, stroke plane inclination angle, greater flap amplitude variation, wider range of flapping frequency variability, etc.) that have yet to be considered.

Acknowledgments

The authors would like to thank the U.S. Air Force Research Laboratories Propulsion Directorate and Campbell Carter for the use of their high frame rate camera. The authors gratefully acknowledge Larry Goss and Jim Crafton of Innovative Scientific Solutions, Inc. (ISSI) for the use of their DPIV 2.0 software. Finally, the authors would like to thank the reviewers for their highly valuable contributions to the improvement of this paper.

References

[1] Jefferies, R, Lt. Col., U.S. Air Force Office of Scientific Research, Air Force Research Laboratories, "Biologically Inspired Flight for Micro Air Vehicles Workshop," [CD-ROM], 21–23 June 2006, Denver, CO.

[2] Taylor, G. S., Schnorbus, T., and Gursul, I., "An Investigation of Vortex Flows Over Low Sweep Delta Wings," AIAA Paper 2003-4021.

[3] Gad-el-hak, M., and Ho, C.-M., "The Pitching Delta Wing," *AIAA Journal*, Vol. 23, No. 11, 1985, pp. 1660–1665.

[4] Riddle, T. W., Wadcock, A. J., Tso, J., and Cummings, R. M., "Experimental Analysis of Vortex Trapping Techniques," *Journal of Fluids Engineering*, Vol. 121, No. 3, 1999, pp. 555–559.

[5] Cox, J., "The Revolutionary Kasper Wing," *Soaring*, Vol. 37, Dec. 1973, pp. 20–23.

[6] Rossow, V. J., "Lift Enhancement by an Externally Trapped Vortex," *Journal of Aircraft*, Vol. 15, No. 9, June 1978, pp. 618–625.

[7] Weis-Fogh, T., "Quick Estimates of Flight Fitness in Hovering Animals, Including Novel Mechanisms for Lift Production," *Journal of Experimental Biology*, Vol. 59, No. 1, 1973, pp. 169–230.

[8] Dickinson, M. H., Lehmann, F.-O., and Sane, S. P., "Wing Rotation and the Aerodynamic Basis of Insect Flight," *Science*, Vol. 284, No. 5422, June 1999, pp. 1954–1960.

[9] Birch, J. M., and Dickinson, M. H., "The Influence of Wing-Wake Interactions on the Production of Aerodynamic Forces in Flapping Flight," *Journal of Experimental Biology*, Vol. 206, No. 13, 2003, pp. 2257–2272.

[10] Dickinson, M. H., and Götz, K. G., "Unsteady Aerodynamic Performance of Model Wings at Low Reynolds Numbers," *Journal of Experimental Biology*, Vol. 174, No. 11, 1993, pp. 45–64.

[11] Birch, J. M., and Dickinson, M. H., "Spanwise Flow and the Attachment of the Leading-Edge Vortex on Insect Wings," *Nature (London)*, Vol. 412, No. 6848, Aug. 2001, pp. 729–733.

[12] Ellington, C. P., Van Den Berg, C., Willmott, A. P., and Thomas, A. L. R., "Leading Edge Vortices in Insect Flight," *Nature (London)*, Vol. 384, No. 6610, Dec. 1996, pp. 626–630.

[13] Bomphrey, R. J., Lawson, N. J., Harding, N. J., Taylor, G. K., and Thomas, A. L. R., "The Aerodynamics of Manduca Sexta: Digital Particle Image Velocimetry Analysis of the Leading-Edge Vortex," *Journal of Experimental Biology*, Vol. 208, No. 6, 2005, pp. 1079–1094.

[14] Gad-el-hak, M., and Ho, C. M., "Unsteady Vortical Flow Around Three-Dimensional Lifting Surfaces," *AIAA Journal*, Vol. 24, No. 5, May 1986, pp. 713–721.

[15] Birch, J. M., Dickson W. B., and Dickinson, M, H., "Force Production and Flow Structure of the Leading Edge Vortex on Flapping Wings at High and Low Reynolds Numbers," *Journal of Experimental Biology*, Vol. 207, No. 7, 2003, pp. 1063–1072.

[16] Maxworthy, T., "The Fluid-Dynamics of Insect Flight," *Annual Review of Fluid Mechanics*, Vol. 13, Jan. 1981, pp. 329–350.

[17] Warrick, D. R., Tobalske, B. W., and Powers, D. R., "Aerodynamics of the Hovering Hummingbird," *Nature (London)*, Vol. 435, No. 7045, June 2005, pp. 1094–1097.

[18] Bilo, D., Lauck, A., and Nachtigall, W., "Measurement of Linear Body Accelerations and Calculation of the Instantaneous Aerodynamic Lift and Thrust in a Pigeon Flying in a Wind Tunnel," Biona-Report 3, Stuttgart, Gustav Fischer Verlag, 1985, pp. 87–108.

[19] Sane, S. P., and Dickinson, M. H., "The Control of Flight Force by a Flapping Wing: Lift and Drag Production," *Journal of Experimental Biology*, Vol. 204, No. 15, 2001, pp. 2607–2626.

[20] Singh, B., Ramasamy, M., Chopra, I., and Leishman, J. G., "Insect-Based Flapping Wings for Micro Hovering Air Vehicles: Experimental Investigations," *American Helicopter Society International Specialists Meeting on Unmanned Rotorcraft: Design, Control and Testing*, American Helicopter Society, Phoenix, AZ, Jan. 2005.

[21] Westerweel, J., "Digital Particle Image Velocimetry—Theory & Application," Delft University Press, Delft, The Netherlands, 1993.

[22] Alford, L., and Altman, A., "Foundation Of A New Investigation Of Natural Flight Characteristics And Theory," AIAA Paper 2005-1357.

[23] Ellington. C. P., "The Novel Aerodynamics of Insect Flight: Applications to Micro-Air Vehicles," *Journal of Experimental Biology*, Vol. 202, No. 23, 1999, pp. 3439–3448.

[24] Lin, J.-C., and Rockwell, D., "Force Identification by Vorticity Fields: Techniques Based on Flow Imaging," *Journal of Fluids and Structures*, Vol. 10, No. 6, Aug. 1996, pp. 663–668.

[25] Lighthill, J., "Fundamentals Concerning Wave Loading on Offshore Structures," *Journal of Fluid Mechanics*, Vol. 173, 1986, pp. 667–681.

[26] Noca, F., Shiels, D., and Jeon, D., "A Comparison of Methods for Evaluating Time-Dependent Fluid Dynamic Forces on Bodies, Using Only Velocity Fields and Their Derivatives," *Journal of Fluids and Structures*, Vol. 13, July 1999, pp. 551–578.

[27] Gharib, M., and Milano, M., "Uncovering the Physics of Flapping Flat Plates with Artificial Evolution," *Journal of Fluid Mechanics*, Vol. 534, July 2005, pp. 403–409.

[28] Huang, M. K., and Chow, C. Y., "Trapping of A Free Vortex by Joukowski Airfoil," AIAA Paper 82-4059, 1982.

[29] Anders. J. B., "Biomimetic Flow Control," AIAA Paper 2000-2543, 2000.

[30] Maxworthy, T., "Experiments on the Weis Fogh Mechanism of Lift Generation by Insects in Hovering Flight. Part 1. Dynamics of the 'Fling," *Journal of Fluid Mechanics*, Vol. 93, No. 1, 1979, pp. 47–63.

[31] Luttges, M., *Accomplished Insect Fliers in Frontiers In Experimental Fluid Mechanics*, edited by M. Gad-El-Hak, Springer, Berlin, 1989, pp. 429–456.

[32] Van Den Berg, C., and Ellington, C. P., "The Three-Dimensional Leading-Edge Vortex of a 'Hovering' Model Hawkmoth," *Philosophical Transactions of the Royal Society of London B*, Vol. 352, No. 1351, March 1997, pp. 329–340.